Aalborg Universitet

Modelling, Analysis, and Design of a Frequency-Droop-Based Virtual Synchronous Generator for Microgrid Applications

Du, Yan; Guerrero, Josep M.; Chang, Liuchen; Su, Jianhui; Mao, Meiqin

Modeling, Analysis, and Design of a Frequency-Droop-Based Virtual Synchronous Generator for Microgrid Applications

Yan Du[1] J. M. Guerrero [2], Liuchen Chang[1,3], Jianhui Su[1], Meiqin Mao[1]

[1] School of Electrical Engineering and Automation, Hefei University of Technology, Hefei, China
[2] Institute of Energy Technology Alborg University, Denmark   joz@et.aau.dk
[3] Dept. of Electrical & Computer Engineering University of New Brunswick

Abstract—In this paper, a power-frequency (*P–ω*) controller is presented for voltage source converters (VSC). The approach is intended for multiple parallel VSCs forming a microgrid operating in both grid-connected and islanded modes. The proposed controller allows a VSC to mimic the operation of a synchronous generator (SG) by implementing the swing equation of SG with a primary frequency controller. In addition, a generalized model of the active power generation dynamics is developed in order to analyze the stability and to design the main control parameters. In contrast with the conventional droop control method, the proposed controller improves the close-loop system dynamic response without changing the frequency accuracy. The obtained results show the good performance of the proposed controller.

Index Terms—parallel converters, primary frequency controller, frequency regulation, inertia, microgrid, droop control.

I. INTRODUCTION

Microgrid is emerging as one of the promising concepts to integrate large-scale distributed resources [1], [2]. A microgrid, also named minigrid, consist of a number of distributed generation systems, energy storage units, and dispersed loads that can operate both autonomously, i.e. in islanded mode, or connected to the grid. Due to this operation flexibility, microgrids can be regarded as important building blocks of next smart grid.

The power electronics interface between the distributed generators, energy storage systems and even loads are normally DC-AC inverters. Those inverters can operate as voltage source converters (VSC), especially in islanded microgrids, since they may fix the frequency or at least to play a role in the frequency regulation [3]. Due to the limited power capacity of an inverter, a number of VSCs operating in parallel may form a microgrid.

Nowadays, droop control is the most widely used controller for VSCs in microgrid applications, since it has been successfully used for controlling parallel uninterruptible power supply systems[4]. In [5], the active and reactive power references are added into the droop method in order to integrate it in a hierarchical control system. Further, with the aim of improving the dynamic performance, a power angle droop control with transient droop characteristic can be used as well [6]. In order to restore the load-dependant frequency, a second frequency control is added for the droop-controlled VSC formed microgrid in [3].

An alternative way to control a VSC is to mimic the dynamic characteristic of a synchronous generator (SG), also called virtual synchronous generator (VSG). For instance, in [8] energy storage plays a similar role as the kinetic energy in the rotor of the SG, so that the dynamic stability of the electrical power system can be improved. In [9], a VSG controller was proposed by using the swing equation of a SG with the purpose of generating the inverter frequency reference. On the other hand, in order to decouple the time-varying mutual fluxes in the ABC reference frame, a controller based on a direct-quadrature-zero (dq0) model of a SG for VSC was presented [10]. However, to the best knowledge of the authors there has not been any comparison between the above two groups of VSC controllers.

In this paper, a VSG-based power-frequency (*P–ω*) controller is proposed by adding a distributed frequency controller (DFC) to the emulated swing equation. This proposed DFC uses the line frequency as a feedback signal that produces an embedded transient active power droop with improved close-loop dynamic performance. In addition, a generalized model for power generation is built in order to illustrate the similarities and differences between the conventional droop control (here abbreviated as *droop control*) and the proposed VSG approach. Results validate the proposed control technique.

II. *P–ω* DROOP CONTROLLER

Fig.1 shows an example of microgrid including a cluster of VSCs consisted of a converter, a LC filter, and a local controller, connected through line impedance to the common bus and distributed loads. The static transfer switch (STS) between the main grid and the microgrid is disconnected from the grid when working in island mode. The VSCs DC links are connected to distributed resources like fuel cells, DC energy storage systems, photovoltaic, and so on.
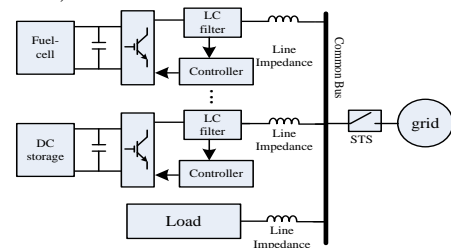

Fig.1 configuration of microgrid system

Considering inductance dominated line impedance, the active power P is predominately dependent on the power angle, while the reactive power Q mostly depends on the output voltage magnitude E. Therefore, *droop control* includes P–ω and Q–E functions. To facilitate hierarchical control of microgrid, the references of active power and reactive power (P^*, Q^*) are added with its control diagram shown in Fig.2.
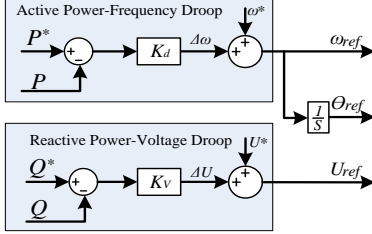

Fig.2 Control diagram of conventional droop control

In Fig.2, the P–ω droop is used to generate the output voltage frequency reference (ω_{ref}) and its rotating angle (θ_{ref}), while the Q–E droop is used to generate output voltage magnitude (U_{ref}). The P–ω *droop control* can be rewritten as:

$$\omega - \omega^* = K_d(P^* - P) \tag{1}$$

with ω^* and P^* being the references of frequency and power, ω and P the output frequency and power of the VSC, and K_d the droop coefficient of the P–ω droop.

Taking into account the low-pass filter of the power measurement, a small signal model of the P–ω droop controller yields to:

$$\hat{\omega} = -\frac{K_d}{\tau s + 1}\hat{P} \tag{2}$$

where ^ denotes a perturbed value, s is the Laplace operator, and τ is the time constant of the low-pass filter. It shows that the P-ω droop controller can low-pass filter the perturbation of the output power P.

III. PROPOSED VSG P–ω CONTROLLER

The swing equation represents the imbalance between the power and the rotating speed in a SG. In [9], the P–ω controller for a VSG is enhanced by adding the swing equation. Since the VSG works around the frequency reference ω^*, the swing equation can be rewritten as

$$P^* - P - D(\omega - \omega^*) = Js(\omega - \omega^*) \tag{3}$$

where P^* and P are the mechanical power and the electromagnetic power of a synchronous generator, J is the inertia momentum, and D is the damping coefficient. In a VSG, P^* and P represents the power reference and the output power. In order to better understand the purpose of the swing equation (3), a small signal analysis can be done as following

$$\frac{\hat{\omega}(s)}{\hat{P}(s)} = \frac{-1}{Js + D} \tag{4}$$

which shows the low-pass filter characteristic relationship between power and frequency variations, according to the swing equation. The time constant can be defined as J/D and the gain is $-1/D$.

By comparing (4) and (3), the VSG without DFC and the *droop-control* can have the same dynamics in small perturbation if the following relationships are satisfied

$$\frac{J}{D} = \tau \quad \text{and} \quad \frac{1}{D} = K_d \tag{5}$$

In this paper, the proposed VSG mimics the dynamic performance of a SG by implementing the SG model and a distributed frequency controller, as shown in Fig.3.
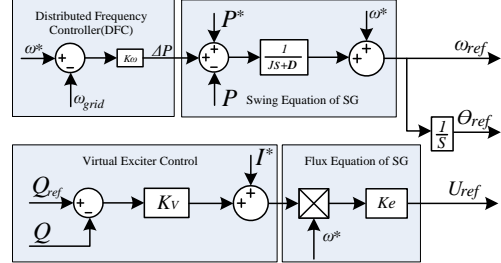

Fig.3. Control diagram of the VSG-based controller.

In Fig.3, the DFC using the line frequency as feedback signal is added to generate the extra incremental power ΔP in order to decrease the frequency perturbation. Therefore, the dynamic power reference is obtained by combining the reference power P^* and ΔP. Coefficient K_ω is the main control parameter of the DFC. Then, the proposed P–ω controller can be expressed as

$$\omega = \frac{1}{Js + D}(P^* - P) + \frac{K_\omega}{Js + D}(\omega^* - \omega_{grid}) + \omega^* \tag{6}$$

which can be seen as two low pass filters applied over power and frequency errors. The static and dynamic performance analysis of this controller is presented in the following subsections.

A. Analysis of Steady-State Performances

In steady state, frequency ω is equal to ω_{grid}, so that (6) can be rewritten as

$$\omega(s) - \omega^*\big|_{s \to 0} = \frac{1}{D + K_\omega}\left[P^* - P(s)\right] \tag{7}$$

The proposed P–ω controller for VSG presented in (7) has similar form of the droop P–ω controller (2). Furthermore, the added DFC increases the value of damping coefficient D in comparison to (5).

B. Analysis of Dynamic Performance

In the proposed VSG, the input signal of the P–ω controller can be divided into two parts commanded by $\omega - \omega_{grid}$ and $\omega^* - \omega$, respectively. Thus the close-loop diagram of the active power response in the VSG can be realized as shown in Fig.4.
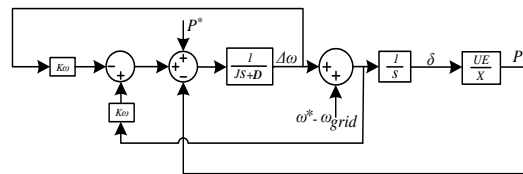

Fig.4. Control structure of VSG-based P-ω controller

In Fig.4, U is the inverter output voltage, E the PCC voltage, and X is the coupling inductance.

Considering the inductance dominated line impedance due to the transformers or the use of LCL filters, the active power can be considered in small-signal sense as proportional to the power angle:

$$P = \frac{UE}{X}\sin\delta \approx \frac{UE}{X}\frac{\omega - \omega_{grid}}{s} \qquad (8)$$

Consequently, the P–ω controller of the VSG can be rewritten as follows:

$$\omega = \frac{1}{Js + D + K_\omega}(P^* - P) + \frac{XK_\omega}{UE}\frac{s}{Js + D + K_\omega}P + \omega^* . \qquad (9)$$

Notice that the first part on the right side of (9) represents a low pass filter over the power deviation, similarly as the droop controllers. However, the second term takes the form of a high-pass filter, which is a derivative term with limited bandwidth applied over the output power P, which only works during the frequency transient.

In case of an islanded microgrid formed by a number of paralleled VSCs, frequency ω_{grid} is determined by all VSCs. Frequency ω differs from ω_{grid} according to the power delivered. As a result, the frequency deviation term, ω–ω_{grid}, in (9) automatically results in a transient frequency droop that enhances the dynamics better than the *droop control* does.

From the above analysis, although both controllers may have the same steady frequency performance, the dynamics of the two controllers may be different due to the dissimilarities between the controller structures.

IV. ACTIVE POWER FLOW ANALYSIS AND MODELING

In this section, a general model of power generation for the *droop control* and the VSG is developed in order to compare their dynamics. In this model, grid frequency ω_{grid} is added as a disturbance due to the disturbance in the grid-frequency of the islanded microgrid. Moreover, measurement filters are added in this model considering their impact over the system dynamics and stability.
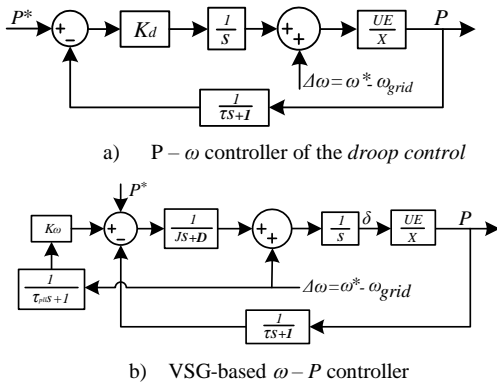The close-loop control diagrams of both controllers are shown in Fig.5

a) P–ω controller of the *droop control*

b)   VSG-based ω–P controller

Fig.5. Block diagram of close-loop system.

Fig. 5 shows that the active power response is generated by two references: *i)* the power reference P^* and *ii)* the grid-frequency deviation $\Delta\omega$. Therefore, the generated output power takes the form:

$$P = G_1(s)P^* + G_2(s)\Delta\omega \qquad (10)$$

where P^* is the power reference, $G_1(s)$ is the transfer function between power reference and output power, $\Delta\omega$ is the frequency deviation, and $G_2(s)$ is the transfer function between the frequency deviation $\Delta\omega$ and the output power. $G_1(s)$ can be defined as the power tracking which indicates the power response for a power reference change, while $G_2(s)$ can be defined as the virtual inertia, which indicates the extra power generated during system frequency changes.

Therefore, the VSC can be modeled as a two-terminal Thévenin equivalent circuit, as shown in Fig.6.
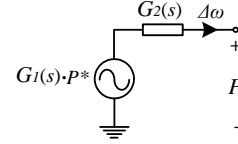

Fig.6 Generalized mode of power generation in VSC.

This electrical model describes the active power generation, which indicates the active power dynamics is determined by $G_1(s)$ and $G_2(s)$. Note that in this equivalent circuit, the voltage represents the power, and the current represents the frequency.

In grid-connected mode, ω_{grid} equals ω^*, the active power dynamics is determined by $G_1(s)$. In islanded mode, ω_{grid} fluctuates, and the active power dynamics is determined by both $G_1(s)$ and $G_2(s)$. Finally, the dynamic analysis is completed by the investigation of $G_1(s)$ and $G_2(s)$ separately. Notice that the power (circuit voltage) droops down when the frequency (circuit current) increases. Consequently, if we want to associate more parallel inverters, the overall equivalent circuit will consist of individual inverters' Thévenin equivalents connected in series. This way the frequency (circuit current) will be common and the power (circuit voltage) will increase when adding more inverters in parallel (circuit series).

V. DYNAMIC PERFORMANCE ANALYSIS

According to the previous analysis, the dynamic power response of the *droop control* cannot be adjusted without changing D and τ parameters. Therefore, it can be used as the baseline to analyze the power dynamics of the proposed VSG. Further, the following assumptions are considered in the dynamic analysis:

1)   The same steady-state droop coefficient (D)

By comparing (1) and (7), it can be concluded that the *VSG* may have the same steady-state frequency as the *droop control* if the following equation is satisfied:

$$\frac{1}{D\omega^* + K_\omega} = K_d \qquad (11)$$

2)   The same power change time-constant (τ)

The time constant of the power change in the *VSG* is determined by the both J and D. By comparing

(2) and (6), the following relationship is satisfied to meet the steady-state requirement

$$\frac{J}{D} = \tau \qquad (12)$$

A. Power tracking transient performance

1) Droop control: The close-loop power tracking control diagram is shown as Fig.7. Then, the transfer function $G_1(s)$ takes the form

$$G_1^{droop} = K_d \frac{UE}{X} \frac{\tau s + 1}{\tau s^2 + s + K_d \frac{UE}{X}} \quad (13)$$

which dynamics is determined by parameters K_d and τ. Their effects have been discussed in [11]. Since K_d is determined by the steady-state control objectives, the dynamics of the power tracking cannot be independently controlled.
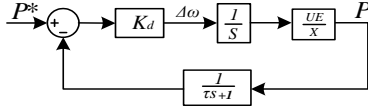

Fig.7. Power tracking close-loop block diagram of the *droop control*

2) VSG: The close-loop power tracking control diagram of the *droop control* is shown as Fig.8.
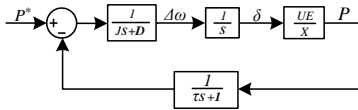

Fig.8 close-loop diagram of power tracking of *VSG*.

In this figure, a low pass filter is added to measure the active power, and τ in the VSG is the time constant of this filter. The transfer function of the *VSG* can be expressed as following:

$$G_1^{VSG}(s) = \frac{\frac{UE}{X}(\tau s + 1)}{J\tau s^3 + (D\tau + J)s^2 + Ds + \frac{UE}{X}} \quad (14)$$

This model shows that the VSG becomes a third order system. The reason of the increase of order is due to the use the power measurement filter. The DFC has no effect on the power tracking performance, while parameters D, J, and τ impact the dynamics of the VSG. According to (11), D decreases when increasing K_ω assuming that the steady-steady maximum frequency deviation requirement is fixed. Therefore, the VSG dynamics can be adjusted without compromising the steady-state performance.

Since the instantaneous power is used to calculate the virtual mechanical power P according to the SG model, reduced time constant for power measurement filter is used. Fig. 9 shows the effect of the time constant (τ) over the dynamics of the VSG. The arrow shows the evolution of the corresponding poles when τ increases. With a smaller τ, s_3 is far away from origin, and s_1 and s_2 become dominants, resulting in an approximated second order system.
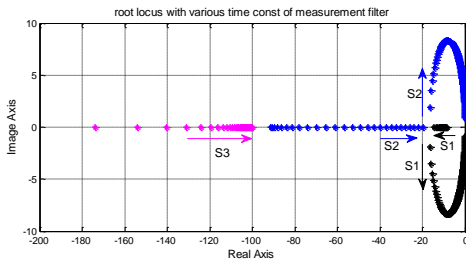

Fig. 9 Family roots of *VSG* for τ variations

Fig. 10 compares the root locus plot of *VSG* and the *droop control* by using the parameters listed in Table I.

Table I
Parameters of Dynamic Analysis

Parameters	Value (Unit)
Nominal Amplitude	220 *(V)*
Voltage Amplitude	220 *(V)*
Droop Coefficient (Kd)	1×10^{-4}
Time constant of LPF(τ)	0.0001-1 *(s)*
Common load	24(*Ω*)
Connecting inductor	1(mH)
Parasitic Resistor	0.15(*Ω*)

In Fig. 10, the droop control considers a variation of τ from 10^{-4} to 1 s, while the VSG has the corresponding value of J, by using (12) for different K_ω values. Notice that both systems can be regarded as a second order system for which the dynamics are mainly determined by the conjugated poles s_1 and s_2. These poles tend to move far away from the real axis, thus becoming complex conjugate poles when τ or J increases, resulting in a more oscillated dynamics.
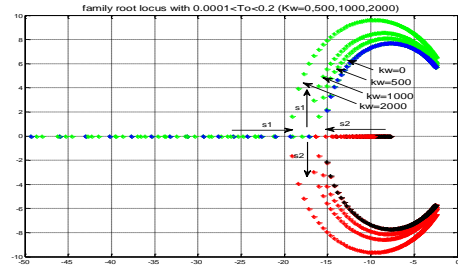

Fig. 10. Root locus of the power tracking performance for the droop control and the VSG, with $0 < K_\omega < 2000$

As Fig. 10 shows, the VSG without using K_ω has the same root locus plot as the *droop control* (blue and black lines). By considering the position of the close-loop zero in both controllers, the droop control has faster dynamics than the VSG due to the larger value of τ in the power measurement. However, the dynamics of the VSG can be improved by increasing K_ω, due to the fact that the separating point of the VSG is moving away from the origin (see Fig. 10).

B. Transient performance of the virtual inertia

Virtual inertia is another mechanism that enables the VSG to inject extra power if the frequency of the grid (ω_{grid}) deviates from the frequency reference.

1) Droop control：The transfer functions of the virtual inertia in case of the *droop control* is given by the following transfer function (see Fig. 11):

$$G_2^{droop} = \frac{\frac{UE}{X}(\tau s + 1)}{\tau s^2 + s + K_d \frac{UE}{X}} \quad (15)$$

Compared to the power tracking transfer function (G_1^{droop}), the transfer function of the virtual inertia (G_2^{droop}) presents the same transient response, except by a smaller gain. Notice that system dynamics cannot be changed in case of the *droop control* if D and τ are selected due to the steady-state requirements.
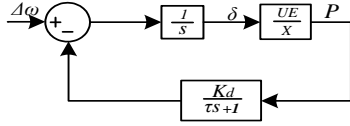
4

Fig. 11. Close-loop block diagram of virtual inertia of Droop

2) VSG: Due to the use of DFC, which uses a phase locked loop (PLL), the VSG has different virtual inertia characteristics. A low pass filter with time constant value of τ_{pll} which models the PLL by approximating it as a first order system, is also added in the frequency measurement in order to investigate its effect on the dynamics behavior. The VSG control diagram is shown in Fig. 12.
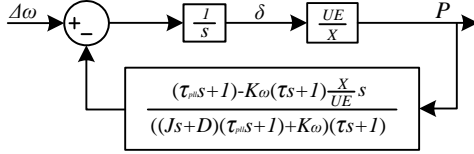

Fig. 12. Close-loop diagram of the virtual inertia of the VSG

From Fig. 12, the transfer function of the virtual inertia in case of the VSG can be derived as follows:

$$G_2^{VSG}(s) = \frac{P_o(s)}{\Delta\omega(s)} = \frac{K_1(\tau s+1)[K_\omega + (Js+D)(\tau_{pll}s+1)]}{s(\tau s+1)(Js+D)(\tau_{pll}s+1) + K_1(\tau_{pll}s+1)} \quad (16)$$

In this case, D changes with K_ω, so that the power response to frequency variations is also dependent on K_ω and τ_{pll}.

Fig. 13 shows the family of root loci considering variations of coefficients K_ω and τ_{pll} from 0 to 0.5. In (16) there are 4 poles associated with virtual inertia. As Fig. 13 shows, s_1 and s_2 are two complex conjugated fixed poles, and s_1 is a real pole moving towards the origin, according to the arrow direction when increasing τ_{pll}. Therefore, s_1 and s_2 are dominant poles with small τ_{pll}, while s_3 becomes dominant for large τ_{pll} values. Besides, the position of s_1 and s_2 is effected by K_ω, i.e. when increasing K_ω, the imagery part of s_1 and s_2 is moving towards the real axis, resulting in a less damped system. Therefore, the larger K_ω and τ_{pll}, the less oscillating the response becomes.
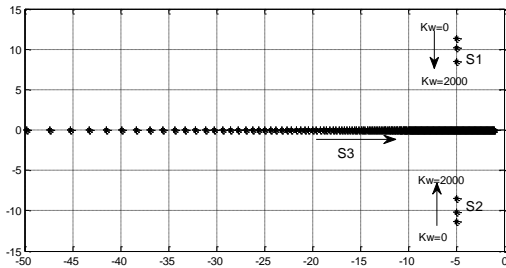
Fig. 13. Family of root loci for *VSG* with τ_{pll} changes and K_ω= 0, 1000, and 2000

With the aim to compare the dynamics of the virtual inertia for both controllers, a family of the root locus plots by using the parameters listed in Table I is shown in Fig. 14. Similarly as in the simulation of the power tracking case, the *droop control* considers a variation of τ from 10^{-4} to 1 s and the VSG has its corresponding

equivalent K_ω and J values.
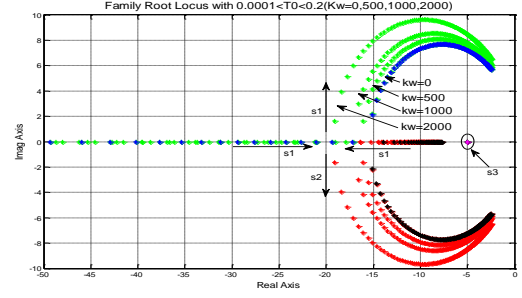
Fig. 14. Family of root loci of the virtual inertia for the *droop control* and the VSG for $0<K_\omega<2000$

In contrast to the *droop control*, in the *VSG* case when increasing K_ω, poles s_1 and s_2 move away from the origin, thus letting s_3 dominant. Therefore, a bigger K_ω leads to a more damped dynamics of the virtual inertia response.

In a practical design, for instant a number of parallel inverters forming an isolated microgrid, it is important to obtain an over-damped power response. However, system dynamics cannot be independently adjusted by the *droop method,* unless K_d is different so that the steady-state performance will be degraded. Therefore, the *droop control* cannot get better dynamics without compromising its stability.

In a sharp contrast, the VSG stability is determined by both D and K_ω parameters, while the transient droop is determined by K_ω. The above analysis shows the dynamics of both the power tracking and the virtual inertia can be adjusted by changing K_ω and τ_{pll} values. The unique control structure of the VSG gives the possibility of optimizing its dynamics without compromising the stability.

VI. SIMULATION RESULTS

The *droop control* and VSG are simulated with the parameters listed in Table I and scheme shown in Fig. 1 for two paralleled inverters. In the case of VSG, K_ω and τ_{pll} are selected to ensure a good transient response, while D and J are adjusted to fulfill the simulation assumption as shown in (11) and (12).

Fig. 15 shows the response of power tracking for various K_ω for the VSG and compares those with the *droop control*. It clearly shows that the VSG has slower dynamic response than the *droop control* for low values of K_ω. The reason is that the zero determined by the value of τ in the *droop control* is closer to the imaginary axis. Thus, the VSG transient response becomes faster and less damped when increasing K_ω because the separating point of the complex-conjugated poles is moving away from the origin.
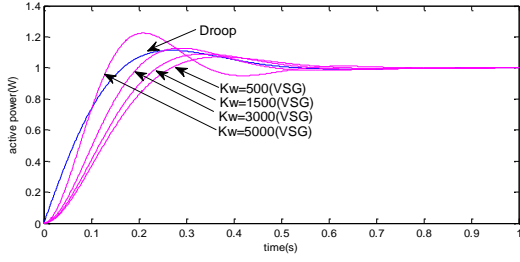
Fig. 15. Dynamic response of power tracking for the *droop control* and the VSG with K_ω variations

Fig. 16 and Fig. 17 show the transient response of the virtual inertia ($P_o/\Delta\omega$) in case of the *droop control* and the *VSG* for different values of K_ω and τ_{pll} separately. Fig. 16 illustrates how the transient response turns more damped and faster when increasing K_ω, since it attracts the two complex-conjugated poles towards the real axis, as shown in Fig. 14. From Fig. 13, this fact also can be explained since the separating point is moving away from the origin. Fig. 17 shows the tendency towards a less oscillatory response when increasing τ_{pll}, since the real pole becomes more dominant, as shown in Fig. 13.
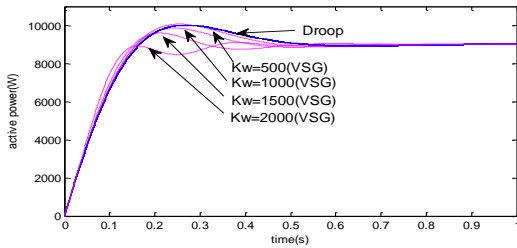

Fig. 16. Dynamic response of the virtual inertia for the *droop control* and the VSG for K_ω variations
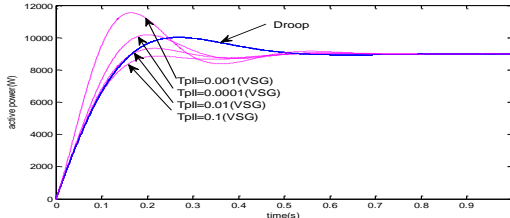

Fig. 17. Dynamic response of the virtual inertia for the *droop control* and the VSG for τ_{pll} variations

In summary, Fig. 15, Fig. 16, and Fig. 17 show that the transient response of the power tracking and the virtual inertia of a VSG can be modified with those parameters, while the transient response of the *droop control* cannot be adjusted without changing K_d and τ. According to the above results, the VSG can obtain a better dynamic performance than the conventional droop control by adjust K_ω and τ_{pll} to get an over-damped fast response for both power tracking and virtual inertia.

In order to verify the dynamic performance of both controllers, an initial phase difference of $0.05rad$ is intentionally settled between both two paralleled inverters. **Error! Reference source not found.** shows the transient active power with the initial phase difference, using *droop* control and *VSG* respectively.
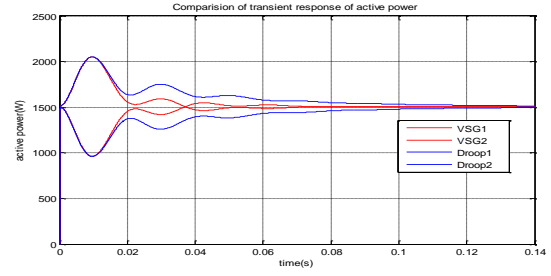

Fig.18 Power transient response of the paralled inverters equipped with *droop control* and VSG

After the initial active power peak due to the initial phase error between inverters, a faster transient response and better dynamic performance are achieved by the VSG, as shown in **Error! Reference source not found.**. These results confirm that the VSG can achieve better power transient response than the *droop* control.

VII. CONCLUSION

A virtual synchronous generator (VSG) based $P–\omega$ controller has been presented in this paper. This $P\text{-}\omega$ controller consist of implementing the swing equation of a synchronous generator (SG) model connected to a distributed frequency controller which can produce a transient frequency droop during transients. The comparison based on a generalized model shows that the proposed controller is able to modify the dynamic response without compromising the steady-state performance by properly tuning the main control parameters. The results show that the dynamic performance is improved in comparison to the conventional droop control.

REFERENCES

[1] B. Kroposki, R. Lasseter, T. Ise, S. Morozumi, S. Papathanassiou, and N. Hatziargyriou, "Making microgrids work," *IEEE Power & Energy Magazine*, 2008, 6(3), pp 40-53.

[2] M. Barnes, J. Kondoh, H. Asano, J. Oyarzabal, G. Ventakaramanan, and R. Lasseter, N. Hatziargyriou, T. Green, "Real-world MicroGrids – An overview," *2007 IEEE International Conference on System of Systems Engineering, SOSE*, 2007, April.

[3] J. M. Guerrero, J. C. Vasquez, J. Matas, L.G. de Vicuna, and M. Castilla, "Hierarchical control of droop-controlled AC and DC microgrids - A general approach toward standardization," *IEEE Trans. Ind. Electron*., vol. 55, no. 1, pp. 158 - 172, Jan. 2011.

[4] T. Kawabata and S. Higashino, "Parallel operation of voltage source inverters," *IEEE Trans. Ind.* Appl.,vol IA-4, pp.281-287, Mar./Apr. 1988.

[5] Y. Li, D. M. Vilathgamuwa, and P.-C. Loh, "Design, analysis and real-time test of a controller for multibus microgrid system," *IEEE Trans. Power Electron.*, 2004,19(5).

[6] J. M. Guerrero, J. Matas, L. G. deVicuna, M. Castilla, and J. Miret, "Wireless-Control Strategy for Parallel Operation of Distributed-Generation Inverters," *IEEE Trans. Ind. Electron.*, vol. 53, no. 5, Oct. 2006, pp. 1461 – 1470.

[7] J. M. Guerrero, J. C. Vasquez, J. Matas, L.G. de Vicuna, and M. Castilla, "Hierarchical control of droop-controlled AC and DC microgrids - A general approach toward standardization," *IEEE Trans. Ind. Electron* ., vol. 55, no. 1, pp. 158 - 172, Jan. 2011

[8] H.-P. Beck and R. Hesse, "Virtual synchronous machine," Electrical Power Quality and Utilisation, *2007, EPQU 2007, 9th International Conference on*.

[9] Q.-C. Zhong and G. Weiss, "Synchronverters: Inverters That Mimic Synchronous Generators," *IEEE Trans. Ind. Electron.*, 2011, 58(4), pp. 1259-1265.

[10] Y. Du, J. Su, and M. Mao, "Autonomous controller based on synchronous generator dq0 model for micro grid inverters," *8th International Conference on Power Electronics*, 2011, May 30-June 3, Shilla Jeju, Korea.

[11] E. A. A. Coelho, P. C. Cortizo, and P. F. D. Garcia, "A Small-signal stability for parallel-connected inverters in stand-alone AC supply systems," *IEEE Trans. Ind. Applicat.,* vol. 38, no. 2, pp. 533-542, Mar/Apr. 2002.